Multi sensor data fusion based approach for the calibration of airdata systems

M. Majeed
majeed_md_123@rediffmail.com
Flight Mechanics and Control Division
CSIR - National Aerospace Laboratories
Bangalore, India

I. N. Kar
ink@ee.iitd.ac.in
Department of Electrical Engineering
Indian Institute of Technology
Delhi, India

ABSTRACT

Accurate and reliable airdata systems are critical for aircraft flight control system. In this paper, both extended Kalman filter (EKF) and unscented Kalman filter (UKF) based various multi sensor data fusion methods are applied to dynamic manoeuvres with rapid variations in the aircraft motion to calibrate the angle-of-attack (AOA) and angle-of-sideslip (AOSS) and are compared. The main goal of the investigations reported is to obtain online accurate flow angles from the measured vane deflection and differential pressures from probes sensitive to flow angles even in the adverse effect of wind or turbulence. The proposed algorithms are applied to both simulated as well as flight test data. Investigations are initially made using simulated flight data that include external winds and turbulence effects. When performance of the sensor fusion methods based on both EKF and UKF are compared, UKF is found to be better. The same procedures are then applied to flight test data of a high performance fighter aircraft. The results are verified with results obtained using proven an offline method, namely, output error method (OEM) for flight-path reconstruction (FPR) using ESTIMA software package. The consistently good results obtained using sensor data fusion approaches proposed in this paper establish that these approaches are of great value for online implementations.

NOMENCLATURE

$C_{z\alpha}$	non dimensional derivative
m	mass of the aircraft
M	Mach number
$\hat{P}^i_{k/k}$	estimated state error covariance of sensor i at kth instant
r_k	diagonal elements of measurement covariance matrix
S	reference area of aircraft
u,v,w	velocity components along the three body-fixed axes
$\bar{u}$	average of inputs at points k and k+1
V	true airspeed
$\hat{x}^i_{k/k}$	estimated state of sensor i at kth instant
Z_k	observation vector

Greek symbols

α	angle-of-attack (AOA)
β	angle-of-sideslip (AOSS)
$dp\alpha$	differential pressure for AOA
$dp\beta$	differential pressure for AOSS
η	additive measurement noise

Paper No. 3629. Manuscript received 14 September 2010, accepted 1 November 2010.

https://doi.org/10.1017/S0001924000005509 Published online by Cambridge University Press

Subscripts

0	initial value
bturb	turbulence in body axes
fs	free stream quantity
fturb	turbulence in flight path axes
g	gust/turbulence quantity
loc_ladt	local measurement from left air data transducer
loc_radt	local measurement from right air data transducer
m	measured quantity
nadt	quantity from nose airdata transducer
npb	quantity from nose probe
nfs	free stream quantity from nose probe.
spb	quantity from side probe
vane	vane measured quantity

Superscripts

m	computation of mean
c	computation of covariance
a	augmented state vector
o	angular unit degree

1.0 INTRODUCTION

One of the aims of airdata systems on aircraft is the determination of flight parameters AOA and AOSS from measurements of local pressures and of local flow angles on wings or fuselage using an appropriate set of sensors. Typical airdata systems include (a) pitot tubes with vanes, (b) multi-function probes, and (c) flush-port airdata systems (FADS). These airdata systems provide measurements of static pressure, total pressure, total temperature, AOA and AOSS[1,3]. These signal measurements are then processed to compute flight control system parameters such as airspeed, dynamic pressure, AOA and AOSS, which are then used as feedback control signals within the flight control architecture. As a result, these signals are flight critical and airdata systems are required on aircraft as part of the flight control system. These airdata sensors installed on high performance modern aircraft must be carefully calibrated to achieve accurate onboard airdata measurements of AOA and AOSS[4,5]. Accuracy of these measurements should be always pursued for a multitude of tasks, including in-flight simulation, flight safety and aircraft performance evaluation, air traffic control, and navigation. These airdata measurements are affected by several flight variables that may vary over a very wide range; thus, airdata sensors calibration must be treated as a multidimensional and nonlinear problem[6,7].

Data compatibility check[8], sometimes called FPR, ensures that the measurements are consistent and error free. For example, the measured AOA must match with that reconstructed from the inertial measurements of accelerations and angular rates. Such verification is possible in the case of flight data because the well-defined kinematic equations of aircraft motion provide a convenient means to bootstrap the information through a numerical procedure. Because no uncertainties are involved in the kinematic model, the compatibility check provides accurate information about the aircraft states. In addition, it provides the estimates of sensitivity factors, zero shifts, and time delays in the recorded data[9,10]. This approach is followed to calibrate the AOA and AOSS from dynamic manoeuvres[2]. Sensitivity factors, biases, and initial conditions are estimated by application of offline method, say OEM[2,9,11].

Online analysis is an attempt to validate the test point before concluding the flight. This procedure using stochastic filtering[12], provides better efficiency and minimises flight test repetitions. Recursive methods have adequate characteristics for online processing. The sensor and the acquisition system characterise the measurement noise, and that should be enough for a FPR problem to provide the input and output covariance noise matrix. Nevertheless, there are some particularities regarding the atmospheric disturbances and the aircraft flexibility, usually not considered in a FPR formulation that requires special treatment. The velocity field within the atmosphere varies in space and time in a random manner, what is called atmospheric turbulence. The airdata sensors, unlike other sensors such as accelerometer and rate gyros, require not only laboratory analysis but also an in-flight calibration. Their responses should be corrected to compensate the disturbances of the air surrounding the aircraft while in flight.

The EKF is a rigorous approach for the nonlinear FPR problem when input and output noises are to be considered. Its solution requires some hypotheses on the system model and noise statistics. System modeling should be done based on physics and engineering experience. Aircraft kinematic modeling is already a well-solved problem. However, noise modelling is a cumbersome task[13] and unfortunately it directly affects filter performance. Strong system nonlinearities, or in other words the higher-order terms neglected in the propagation of states and error covariances, and wrong values of noise statistics may result in biased estimates and in the worst-case lead to divergence[14]. In contrast to the first order approximation used in the EKF for covariance propagation, in the UKF, a finite set of points, called sigma points, are propagated through nonlinear dynamics without approximations. The flaw in the EKF of calculating mean and covariance of random variables undergoing a nonlinear transformation is thus eliminated in the UKF. This difference leads to a better performance of the UKF, which is shown to be equivalent to the second order EKF, but without calculating the Jacobian or Hessian. This characteristic, namely propagation, does not require computations of first or higher-order approximations of system functions, which together with the resulting improved performance makes it better suited for real time applications[15].

A recent research study uses a detailed aerodynamic model of the aircraft within an EKF framework[16] offers the potential to eliminate the sensors required to measure AOA and AOSS. Today's modern computers have the computational throughput to functionally estimate these parameters accurately, thus eliminating these sensors, or at a minimum providing a functional backup for improved reliability. Unfortunately, there is no way to use such estimation framework prior to the validation of aerodynamic database consisting of force and moment coefficients, because estimation accuracy is directly tied to the aerodynamic data base accuracy[16]. This is because the models of aerodynamic forces, propulsive forces, and moments are embedded in the EKF formulation. So, measurements of AOA and AOSS are primary requirements for the aircraft, which is new or which does not have a validated aerodynamic database. For an angle with multiple sensors, sensor fusion algorithms yield good results since the fusion of data from multiple sensors results in both qualitative and quantitative benefits[17-19].

Moreover, the effectiveness of another Kalman Filter (KF) algorithm incorporating GPS[2,20] for real time airdata calibration is directly dependent on the GPS error as it uses differential GPS (DGPS) position and velocity data for the measurements in framework. GPS has the advantages of all weather, globality and consistently high precision. But data update rate of a GPS receiver is low (normally at 1Hz) and the performance is dependent on the number and geometry of satellites being tracked. In comparison, the proposed approach in our paper overcomes this deficiency because multiple airdata sensors outputs are taken as measurements. By fusing valuable information from sensors into the EKF algorithm helps in estimating each sensor's calibration parameters separately in terms of sensor offset error and sensitivity factor.

Fusion processes are often categorised as low, intermediate or high level fusion depending on the processing stage at which fusion takes place. Low-level fusion, also called data fusion, combines several sources of raw data to produce new raw data that is expected to be more informative and synthetic than the inputs. There are two approaches for fusion of multiple sensor data: measurement fusion

https://doi.org/10.1017/S0001924000005509 Published online by Cambridge University Press

and state vector fusion (SVF). In measurement fusion, sensor measurements are combined and an optimal estimate of target state vector is obtained. Since this approach is optimal, it is theoretically superior. Currently there exist two commonly used measurement fusion methods for KF based multi sensor data fusion. The first measurement fusion (MF-I) simply merges the multi sensor data through the observation vector of the KF, whereas the second measurement fusion (MF-II) combines the multi sensor data based on a minimum mean square error criterion. But for various reasons, measurement fusion may not be practical for field implementation. This is so because volume of the sensor data to be transmitted to the fusion center from different stations could overwhelm the capacity of the existing data links among those stations[19]. For this reason, SVF is preferable for implementation in a variety of practical systems. It has been pointed out that SVF methods are only effective when the KF are consistent[18], which restricts the practical applications of SVF methods. Many realistic applications are often nonlinear and the consequent KF are based on linearised process models and usually are inconsistent due to the model errors introduced by the linearisation process. This motivates the use of the UKF for the SVF, because it determines the mean and covariance accurately to the second order.

The primary aim of the presented data fusion approach for airdata calibration is to accurately estimate airdata parameters or to make inferences that may not be feasible from a single sensor alone as in FPR using EKF[8,13]. In addition, reduced ambiguity, increased confidence and improved system reliability are the main benefits applicable to majority of the data fusion applications. The main contribution of this work is to online estimate, AOA and AOSS using various multi sensor data fusion methods within both EKF and UKF framework, aiming at an online application and to compare the relative performance of each method within different framework. In our approach, we have also given special attention to the presence of turbulence during the flight manoeuvres. These methods are applied to flight data of a high performance fighter aircraft. Major contribution occurs in situations where there is a significant sensors noise property variation. FPR using OEM is also applied to analyse the flight manoeuvres and to calibrate AOA and AOSS using ESTIMA[21]. It helps to reconfirm the results obtained from KF based sensor fusion real time approach, by comparing these results with this standard method[11].

In the following section, the sensor fusion approaches are applied to dynamic manoeuvres with rapid variations in the aircraft motion to calibrate the flow angles. Section 2 briefly explains the EKF and UKF, and Section 3 represents the proposed KF based multi sensor data fusion approaches. Section 4 describes system dynamic and measurement models, and the following one represents the measurement model. The validation using simulated and flight test data is performed in Section 5 and conclusions are drawn in Section 6.

2.0 STATE AND PARAMETER ESTIMATION USING KALMAN FILTER

One of the most popular forms of representing aircraft equations of motion in the time domain is the state space form[22]. The dynamic and measurement model is assumed to be described by the following continuous-discrete state space models:

$$\dot{\mathbf{x}}(t) = \mathrm{f}(\mathbf{x}(t), \mathbf{u}(t), \mathbf{w}(t))$$
$$\mathbf{y}(t) = \mathrm{h}(\mathbf{x}(t)) \quad \mathbf{z}(k) = \mathbf{y}(k) + \mathbf{v}(k) \quad \mathbf{x}(0) = \mathbf{x}_0 \qquad \ldots (1)$$

Functions $\mathbf{f} \in \Re^n$ and $\mathbf{h} \in \Re^m$ are general nonlinear functions; vector $\mathbf{x} \in \Re^n$ is the state vector; $\mathbf{u} \in \Re^1$ is the input/control vector; $\mathbf{y} \in \Re^m$ is the output vector, and $\mathbf{z} \in \Re^m$ is sampled at discrete points with a uniform Δt sampling time; vectors $\mathbf{w}$ and $\mathbf{v}$ are process and measurement noises and have covariance matrices $\mathbf{Q}$ and $\mathbf{R}$, respectively. More precisely, noises are considered to be zero mean, white, and with Gaussian distribution. They are also assumed to be independent between themselves and also with respect to the initial condition $x(0)$, that is,

$$E\{\mathbf{w}(k)\} = 0 \quad E\{\mathbf{v}(k)\} = 0 \quad E\{\mathbf{w}(k)\mathbf{w}(j)^T\} = \mathbf{Q}\delta(k-j)$$
$$E\{\mathbf{v}(k)\mathbf{v}(j)^T\} = \mathbf{R}\delta(k-j) \qquad E\{\mathbf{w}(k)\mathbf{v}(j)^T\} = 0$$
$$E\{\mathbf{x}(0)\mathbf{w}(k)^T\} = 0 \qquad E\{\mathbf{x}(0)\mathbf{v}(k)^T\} = 0 \qquad \ldots (2)$$

Measured flight data can contain considerable amount of noise, furthermore there might be biases and unobserved states in the system model which must be estimated; hence filtering techniques are generally employed. The most popular nonlinear filtering technique is the extended Kalman filter (EKF) and their details are not described here for brevity, and they are illustrated in Ref. 23 and 24. Although widely used, EKFs have some deficiencies, including the requirement of differentiability of the state dynamics as well as susceptibility to bias, hard to tune and implement when dealing with significant nonlinearities and exhibits divergence in estimates. Unscented Kalman filter, on the contrary, uses the nonlinear model directly instead of linearising it[15].

The UKF was developed with the underlying assumption that approximating a Gaussian distribution is easier than approximating a nonlinear transformation. The UKF uses deterministic sampling to approximate the state distribution as a Gaussian random variable (GRV). The sigma points are propagated through the nonlinear system. The posterior mean and covariance are then calculated from the propagated sigma points. The UKF determines the mean and covariance accurately to the second order, while the EKF is only able to obtain first order accuracy. Therefore, the UKF provides better state estimates for nonlinear systems.

To implement the UKF, it is necessary to define $(2n_a + 1)$ sigma points, where n_a is the total number of states to be estimated, which include the basic system state, the unknown system parameters, as well as the process and measurement noise disturbances. One of the sigma vectors is the expected value of the augmented state vector, and the remaining $2n_a$ points are obtained from the columns of the matrix square root $\pm(\gamma P)$ for $i = 1,2, \ldots, n$ where $\mathbf{P}$ is the covariance matrix of the augmented state vector $\mathbf{x_a}$, $\gamma = \sqrt{(n_a + \lambda)}$ and $\gamma = \alpha_1^2(n_a + \kappa) - n_a$ are scaling parameters. The constant α_1 determines the spread of the sigma points around the estimated $\mathbf{x_a}$; it is set equal to small positive value of less than 1 and $\kappa = 0$ or $3 - n_a$ for state or parameter estimation[11].

The weights required in the computation of mean and covariance are defined as

$$W_0^m = \lambda/(n_a + \lambda); \quad W_0^c = \lambda/(n_a + \lambda) + (1 - \alpha_1^2 + \beta_1);$$
$$W_i^m = W_i^c = 1/\{2(n_a + \lambda)\}, \quad i = 1,2,\ldots,2n_a \qquad \ldots (3)$$

where the subscripts '0' corresponds to the estimated states and $i = 1,2, \ldots 2n_a$ the other sigma points. The constant β_1 is used to incorporate prior knowledge of distribution of x in the computation of weights for covariances W_0^c; the optimum value is $\beta_1 = 2$ for Gaussian distribution. The augmented state vector of the size $(n_a \times 1)$ is given by

$$\mathbf{x_k^a} = \begin{bmatrix} \mathbf{x_k^T} & \mathbf{\Theta_k^T} & \mathbf{w_k^T} & \mathbf{v_k^T} \end{bmatrix}^{\mathbf{T}} \qquad \ldots (4)$$

where Θ_k the $(n_q \times 1)$ vector of unknown parameters and $n_a = n_x + n_q + n_w + n_v$.

Pseudo-code for unscented Kalman filter

● Initialisation

$$\hat{\mathbf{x}}_0^{\mathbf{a}} = \mathbf{E}\{\mathbf{x}_0^{\mathbf{a}}\} = \mathbf{E}\{\begin{bmatrix} \hat{\mathbf{x}}_0^{\mathbf{T}} & \mathbf{\Theta}^{\mathbf{T}} & \mathbf{w}_0^{\mathbf{T}} & \mathbf{v}_0^{\mathbf{T}} \end{bmatrix}\} = \begin{bmatrix} \hat{\mathbf{x}}_0^{\mathbf{T}} & \mathbf{\Theta}_0^{\mathbf{T}} & 0 & 0 \end{bmatrix} \qquad \ldots (5)$$

https://doi.org/10.1017/S0001924000005509 Published online by Cambridge University Press

$$\mathbf{P}_0^a = \mathbf{E}\left\{(\mathbf{x}_0^a - \hat{\mathbf{x}}_0^a)(\mathbf{x}_0^a - \hat{\mathbf{x}}_0^a)^{\mathrm{T}}\right\} = \begin{bmatrix} \mathbf{P}_{x_0} & 0 & 0 & 0 \\ 0 & \mathbf{P}_{\Theta_0} & 0 & 0 \\ 0 & 0 & \mathbf{Q} & 0 \\ 0 & 0 & 0 & \mathbf{R} \end{bmatrix} \quad \ldots (6)$$

1. Set discrete time point $k = 1$
2. Calculate the $(2n_a + 1)$ sigma points:

$$\tilde{\boldsymbol{\chi}}_{\mathbf{k}}^{\mathbf{a}} = \left[\hat{\mathbf{x}}_{\mathbf{k}}^{\mathbf{a}} \quad \hat{\mathbf{x}}_{\mathbf{k}}^{\mathbf{a}} - \gamma\sqrt{\hat{\mathbf{P}}_{\mathbf{k}}^{\mathbf{a}}} \quad \hat{\mathbf{x}}_{\mathbf{k}}^{\mathbf{a}} + \gamma\sqrt{\hat{\mathbf{P}}_{\mathbf{k}}^{\mathbf{a}}}\right] \quad \ldots (7)$$

3. Compute the predicted (time updated) states and covariances:

$$\tilde{\boldsymbol{\chi}}_{\mathbf{k+1}}^{\mathbf{a}} = \hat{\boldsymbol{\chi}}_{\mathbf{k}}^{\mathbf{a}}(k) + \int_{t_k}^{t_{k+1}} \mathbf{f}\left[\boldsymbol{\chi}^{\mathbf{a}}(t), \bar{\mathbf{u}}(k)\right] \mathrm{d}t \quad \ldots (8)$$

$$\tilde{\mathbf{x}}_{\mathbf{k+1}} = \sum_{i=0}^{2n_a} W_i^m \tilde{\boldsymbol{\chi}}_{\mathbf{i,k+1}}^{\mathbf{a}} \quad \ldots (9)$$

$$\tilde{\mathbf{P}}_{\mathbf{k+1}} = \sum_{i=0}^{2n_a} W_i^c \left[\tilde{\boldsymbol{\chi}}_{\mathbf{i,k+1}}^{\mathbf{a}} - \tilde{\mathbf{x}}_{\mathbf{k+1}}\right]\left[\tilde{\boldsymbol{\chi}}_{\mathbf{i,k+1}}^{\mathbf{a}} - \tilde{\mathbf{x}}_{\mathbf{k+1}}\right]^T \quad \ldots (10)$$

4. Perform the measurement update:

$$\mathbf{Y}_{\mathbf{k+1}} = \mathbf{h}\left[\tilde{\boldsymbol{\chi}}_{\mathbf{k+1}}^{\mathbf{x}}, \tilde{\boldsymbol{\chi}}_{\mathbf{k+1}}^{\mathbf{v}}\right] \quad \ldots (11)$$

$$\tilde{\mathbf{y}}_{\mathbf{k+1}} = \sum_{i=0}^{2n_a} W_i^m \mathbf{Y}_{\mathbf{i,k+1}} \quad \ldots (12)$$

$$\mathbf{P}_{\tilde{\mathbf{y}}\tilde{\mathbf{y}}_{\mathbf{k+1}}} = \sum_{i=0}^{2n_a} W_i^c \left[\mathbf{Y}_{\mathbf{i,k+1}} - \tilde{\mathbf{y}}_{\mathbf{k+1}}\right]\left[\mathbf{Y}_{\mathbf{i,k+1}} - \tilde{\mathbf{y}}_{\mathbf{k+1}}\right]^T \quad \ldots (13)$$

$$\mathbf{P}_{\tilde{\mathbf{x}}\tilde{\mathbf{y}}_{\mathbf{k+1}}} = \sum_{i=0}^{2n_a} W_i^c \left[\tilde{\boldsymbol{\chi}}_{\mathbf{i,k+1}}^{\mathbf{x}} - \tilde{\mathbf{x}}_{\mathbf{k+1}}\right]\left[\mathbf{Y}_{\mathbf{i,k+1}} - \tilde{\mathbf{y}}_{\mathbf{k+1}}\right]^T \quad \ldots (14)$$

$$\mathbf{K}_{\mathbf{k+1}} = \mathbf{P}_{\tilde{\mathbf{x}}\tilde{\mathbf{y}}_{\mathbf{k+1}}} \mathbf{P}_{\tilde{\mathbf{y}}\tilde{\mathbf{y}}_{\mathbf{k+1}}}^{-1} \quad \ldots (15)$$

$$\hat{\mathbf{x}}_{\mathbf{k+1}} = \tilde{\mathbf{x}}_{\mathbf{k+1}} + \mathbf{K}_{\mathbf{K+1}}(\mathbf{z}_{\mathbf{k+1}} - \tilde{\mathbf{y}}_{\mathbf{k+1}}) \quad \ldots (16)$$

$$\hat{\mathbf{P}}_{\mathbf{k+1}} = \tilde{\mathbf{P}}_{\mathbf{k+1}} - \mathbf{K}_{\mathbf{K+1}} \mathbf{P}_{\tilde{\mathbf{y}}\tilde{\mathbf{y}}_{\mathbf{k+1}}} \mathbf{K}_{\mathbf{k+1}}^{\mathbf{T}} \quad \ldots (17)$$

5. Increment k and jump back to step 2 to continue.

$\boldsymbol{\chi}^a = \left[(\boldsymbol{\chi}^x)^T (\boldsymbol{\chi}^w)^T (\boldsymbol{\chi}^v)^T\right]$ denotes the sigma points, χ^x corresponds to the system states and unknown parameters.

3.0 PROPOSED APPROACH FOR CALIBRATION OF AIRDATA SYSTEMS

The proposed procedure is a KF-based multi sensor data fusion algorithm, which is applied to dynamic manoeuvres (say doublet, 3211, pull up and AOA sweep) with rapid variations in the aircraft motion to calibrate AOA and AOSS.

3.1 Sensor fusion algorithms

Methods for KF based data fusion, including SVF and measurement fusion, have been widely studied over the last decade[25,27]. As shown in Fig.1(a), SVF methods use a group of KF to obtain individual sensor-based state estimates, which are then fused to obtain an improved joint state estimate. Whereas measurement fusion methods directly fuse the sensor measurements to obtain a weighted or combined measurement and then use a single KF to obtain the final state estimate based upon the fused observation. Measurement fusion methods generally provide better overall estimation performance, while SVF methods have a lower computation and communication cost and have the advantages of parallel implementation and fault-tolerance.

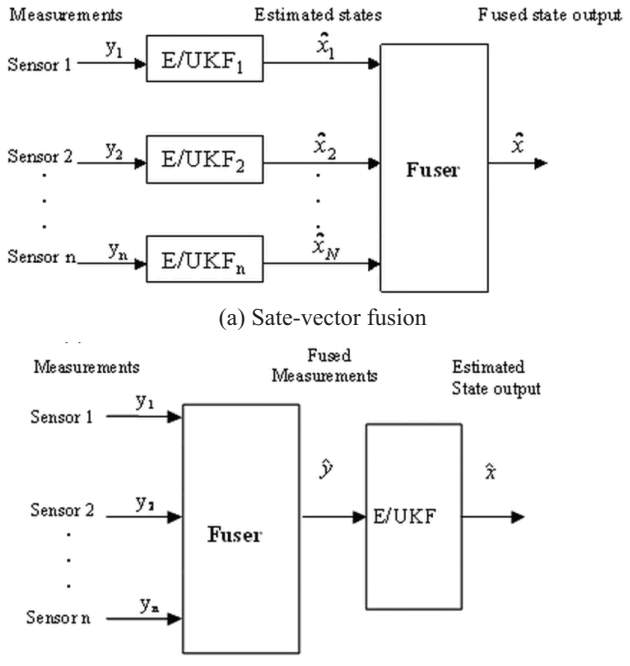

(a) Sate-vector fusion

(b) Measurement fusion

Figure 1. Extended/unscented Kalman-filter-based multi sensor data fusion.

Aircraft equation of motion is represented in Equation (1) but measurement equation for sensors i and j is given by $\mathbf{Z}_k^m = \mathbf{c}_k^m \mathbf{x}_k^m + \mathbf{v}_k^m$, $m = i,j$ where $\mathbf{z}_k$ is the measurement at time k and ν_k is measurement noise with

$$E(\mathbf{v}_k^m) = 0; \quad E(\mathbf{v}_k^m \mathbf{v}_l^m) = \mathbf{r}_k^m \delta_{kl}; \quad E(\mathbf{v}_k^i \mathbf{v}_l^j) = 0$$

Fusion of these sensors can now take place at either the state vector or measurement level.

3.1.1 State vector fusion

In SVF, state and state error covariance estimates of KF for each of the sensors are then used to obtain the fused state according to the following equations[28]. Fused state and covariance of fused state are given by Equations (18) and (19) respectively.

$$\hat{\mathbf{x}}_{\mathbf{k/k}}^{\mathbf{F}} = \hat{\mathbf{x}}_{\mathbf{k/k}}^{\mathbf{i}} + \hat{\mathbf{P}}_{\mathbf{k/k}}^{\mathbf{i}}\left[\hat{\mathbf{P}}_{\mathbf{k/k}}^{\mathbf{i}} + \left(\hat{\mathbf{P}}_{\mathbf{k/k}}^{\mathbf{j}}\right)^{\mathbf{T}}\right]^{-1}\left(\hat{\mathbf{x}}_{\mathbf{k/k}}^{\mathbf{j}} - \hat{\mathbf{x}}_{\mathbf{k/k}}^{\mathbf{i}}\right) \quad \ldots (18)$$

$$\hat{\mathbf{P}}_{\mathbf{k/k}}^{\mathbf{F}} = \hat{\mathbf{P}}_{\mathbf{k/k}}^{\mathbf{i}} + \hat{\mathbf{P}}_{\mathbf{k/k}}^{\mathbf{i}}\left[\hat{\mathbf{P}}_{\mathbf{k/k}}^{\mathbf{i}} + \left(\hat{\mathbf{P}}_{\mathbf{k/k}}^{\mathbf{j}}\right)^{\mathbf{T}}\right]^{-1}\left(\hat{\mathbf{P}}_{\mathbf{k/k}}^{\mathbf{i}}\right)^{\mathbf{T}} \quad \ldots (19)$$

In this case, the common process noise affecting the target dynamics corresponding to each of sensors is assumed to be negligible.

https://doi.org/10.1017/S0001924000005509 Published online by Cambridge University Press

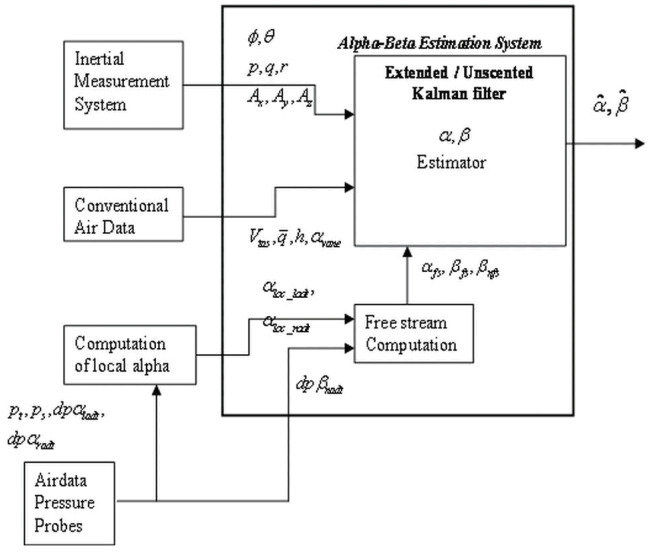

Figure 2. Alpha-Beta Estimation Scheme.

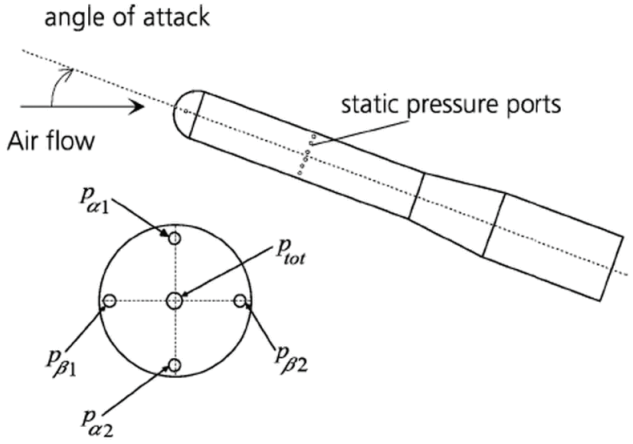

Figure 3. Five hole probe: port configuration.

3.1.2 Measurement fusion method I

The MF-1 integrates the sensor measurement information by augmenting the observation vector as follows.

$$\mathbf{z_k} = \mathbf{z_k^{(I)}} = \begin{bmatrix} \mathbf{z_k^i} & \mathbf{z_k^j} \end{bmatrix}^{\mathbf{T}} \quad \ldots (20)$$

$$\mathbf{r_k} = \mathbf{r_k^{(I)}} = \mathbf{diag}\begin{bmatrix} \mathbf{r_k^i} & \mathbf{r_k^j} \end{bmatrix}^{\mathbf{T}} \quad \ldots (21)$$

3.1.3 Measurement fusion method II

The MF-II obtains the fused measurement information by weighted observation as[23]:

$$\mathbf{z_k} = \mathbf{z_k^{(II)}} = \mathbf{z_k^i} + \mathbf{r_k^i}\left[\mathbf{r_k^i} + \left(\mathbf{r_k^j}\right)^{\mathbf{T}}\right]^{-1}\left(\mathbf{z_k^j} - \mathbf{z_k^i}\right) \quad \ldots (22)$$

$$\mathbf{r_k} = \mathbf{r_k^{(I)}} = \mathbf{r_k^i} - \mathbf{r_k^i}\left[\mathbf{r_k^i} + \left(\mathbf{r_k^j}\right)^{\mathbf{T}}\right]^{-1}\left(\mathbf{r_k^i}\right)^{\mathbf{T}} \quad \ldots (23)$$

In the presence of wind or atmospheric disturbances, a single sensor doest not give the optimum result due to its discrepancy with true value, but more than one sensor will do the task through integration (fusion) of information with the application of KF algorithm. The flow distortion at fuselage and wings of the aircraft make sensing device even more complex and provides the local measurements, which need to convert in free stream. Under these situations, measurement errors are accumulated, if no corrections are applied and free stream computation provides this correction in a nominal way. To solve this problem, KF based sensor fusion approach by using measurements at various sensors for AOA (vane deflection, side pressure probe) and AOSS (side pressure probe and nose pressure probe), together with free stream computation of AOA and AOSS is proposed and is unlike KF algorithm incorporating GPS[2,20]. This procedure is similar to flight path reconstruction using EKF, wherein the fusion of data from multiple flow angle sensors results in both qualitative and quantitative benefits. The comparison study of different fusion algorithms are made within the framework of both EKF and UKF.

3.2 Alpha-Beta estimation algorithm

The main goal of the investigations is to obtain online accurate flow angles from the data measured by both vane and multifunction airdata probes even with the adverse effect of wind or turbulence. The investigations are made with both simulated and flight test data of a high performance aircraft. The schematic block diagram of Alpha-Beta Estimation Scheme is shown in Fig. 2.

Multi-function five-hole pressure probe (Fig. 3) provides measurements of total pressure p_{tot}, differential pressures $p_{\alpha 1} - p_{\alpha 2}(=\mathrm{d}p\alpha_{ladt},\mathrm{d}p\alpha_{radt})$ for AOA and $p_{\beta 1} - p_{\beta 2}(=\mathrm{d}p\beta_{nadt})$ for AOSS. The static pressure p_s also measured very close to the tip of the nose boom. There are two local measurements (α_{loc_ladt},α_{loc_radt}) from pressure probes on left and right sides, which are given by

$$\alpha_{loc\_ladt} = \frac{\mathrm{d}p\alpha_{ladt}}{K\left(p_t - p_s\right)} \quad \text{and} \quad \alpha_{loc\_radt} = \frac{\mathrm{d}p\alpha_{radt}}{K\left(p_t - p_s\right)} \quad \ldots (24)$$

where $(p_t - p_s)$ is dynamic pressure, K = $f(mach)$ is the sensitivity coefficient specified by the manufacturer[2]. Each local measurement is a function of free stream values alpha, beta and Mach. The free stream flow angles (α_{fs}, β_{fs}) are inversely functions of mach and two local measurements of pressure probes at both sides,

$$\begin{aligned} \alpha_{fs} &= f_1(M, \alpha_{loc\_ladt}, \alpha_{loc\_radt}) \\ \text{and} \quad \beta_{fs} &= f_2(M, \alpha_{loc\_ladt}, \alpha_{loc\_radt}) \end{aligned} \quad \ldots (25)$$

Other KF measurements are, corrected vane deflection AOA (α_{vane}) accounted by position error correction from digital flight control computer using wind tunnel facility and free stream beta from nose probe (β_{nfs}) as shown in the Fig. 2. The free stream nose probe beta is directly computed through functional look up table with the differential pressure ($\mathrm{d}p\beta_{nadt}$) for AOSS. The concept of considering the vane deflection AOA corrected through position error correction is to estimate the discrepancy in measurement in terms of sensitivity factor and offset error, associated with use of scaled version aircraft at wind tunnel test facility where does not have process disturbance like gust or turbulence.

4.0 SYSTEM DYNAMIC AND MEASUREMENT MODELS

To summarise the system dynamic and measurement models, it must be noted that all calibration parameters are considered as random walk and incorporated into the state vector, via state augmentation. These groups of first order differential equations are necessary to

https://doi.org/10.1017/S0001924000005509 Published online by Cambridge University Press

characterise the aircraft motion and are available in most of the text books[24]. The full kinematic model is represented by

$$\begin{aligned}
\dot{u} &= -(q_m - \Delta q)w + (r_m - \Delta r)v - g\ \mathrm{Sin}\theta + A_x^{CG},\ u(t_0) = u_0 \\
\dot{v} &= -(r_m - \Delta r)u + (p_m - \Delta p)w + g\ \mathrm{Cos}\theta\ \mathrm{Sin}\phi + A_y^{CG}, \quad v(t_0) = v_0 \\
\dot{w} &= -(p_m - \Delta p)v + (q_m - \Delta q)u + g\ \mathrm{Cos}\phi\ \mathrm{Cos}\theta + A_z^{CG}, \quad w(t_0) = w_0 \\
\dot{\phi} &= (p_m - \Delta p) + (q_m - \Delta q)\ \mathrm{Sin}\phi\ \mathrm{Tan}\theta + (r_m - \Delta r)\ \mathrm{Cos}\phi\ \mathrm{Tan}\theta, \quad \phi(t_0) = \phi_0 \\
\dot{\theta} &= (q_m - \Delta q)\ \mathrm{Cos}\phi - (r_m - \Delta r)\ \mathrm{Sin}\phi, \quad \theta(t_0) = \theta_0 \\
\dot{h} &= u\ \mathrm{Sin}\theta - v\ \mathrm{Sin}\phi\ \mathrm{Cos}\theta - w\ \mathrm{Cos}\phi\ \mathrm{Cos}\theta, \quad h(t_0) = h_0
\end{aligned} \quad \ldots (26)$$

where p, q, and r are the projection of the angular rate vector along the aircraft body axis and their biases in measurements are defined by (Δp, Δq, Δr); θ and ϕ are, respectively, the pitch and the roll angles; u, v, w are inertial speed projections along the aircraft body axis. The linear accelerations (A_x^{CG}, A_y^{CG}, A_z^{GC}) at the center of gravity (CG) are computed from the accelerations (A_{xm}^{AS}, A_{ym}^{AS}, A_{zm}^{AS}) measured by the acceleration sensor at a point away from the CG through the following relation[24]:

$$\begin{aligned}
A_x^{CG} &= a_{xm}^{AS} + (q^2 + r^2)x_{ASCG} - (pq - \dot{r})y_{ASCG} - (pr + \dot{q})z_{ASCG} - \Delta A_x \\
A_y^{CG} &= a_{ym}^{AS} + (pq + \dot{r})x_{ASCG} + (p^2 + r^2)y_{ASCG} - (qr - \dot{p})z_{ASCG} - \Delta A_y \\
A_z^{CG} &= a_{zm}^{AS} - (pr - \dot{q})x_{ASCG} - (qr + \dot{p})y_{ASCG} + (p^2 + q^2)z_{ASCG} - \Delta A_z
\end{aligned} \quad \ldots (27)$$

Here (x_{ASCG}, y_{ASCG}, z_{ASCG}) denote the position of the accelerometer with respect to the CG in the body-fixed co-ordinates; the biases in the measurement of (A_{xm}^{AS}, A_{ym}^{AS}, A_{zm}^{AS}) are denoted by (ΔA_x, ΔA_y, ΔA_z).

The measurement equations are given by:

$$\begin{aligned}
V_m &= \sqrt{u^2 + v^2 + w^2} + \eta_v \\
\bar{q}_m &= \frac{1}{2}\rho\left(u^2 + v^2 + w^2\right) + \Delta\bar{q} + \eta_{\bar{q}} \\
\phi_m &= \phi + \eta_\phi \\
\theta_m &= \theta + \eta_\theta \\
h_m &= h + \eta_h \\
\alpha_{vane} &= K_{\alpha_{vane}}\mathrm{Tan}^{-1}\left(\frac{w_{vane}}{u_{vane}}\right) + \Delta\alpha_{vane} + \eta_{\alpha_{vane}} \\
\alpha_{spb} &= K_{\alpha_{spb}}\mathrm{Tan}^{-1}\left(\frac{w_{spb}}{u_{spb}}\right) + \Delta\alpha_{spb} + \eta_{\alpha_{spb}} \\
\beta_{spb} &= K_{\beta_{spb}}\mathrm{Sin}^{-1}\left(\frac{v_{spb}}{\sqrt{u_{spb}^2 + v_{spb}^2 + w_{spb}^2}}\right) + \Delta\beta_{spb} + \eta_{\beta_{spb}} \\
\beta_{npb} &= K_{\beta_{npb}}\mathrm{Sin}^{-1}\left(\frac{v_{npb}}{\sqrt{u_{npb}^2 + v_{npb}^2 + w_{npb}^2}}\right) + \Delta\beta_{npb} + \eta_{\beta_{npb}}
\end{aligned} \quad \ldots (28)$$

The density of air ρ can be computed from the actual measurement of static pressure p_s using the universal gas law, $\rho = p_s / RT_s$, where R is the gas constant and T_s the static temperature. $K_{\alpha_{vane}}$, $K_{\alpha_{spb}}$, $K_{\beta_{spb}}$, $K_{\beta_{npb}}$ are the scale factors and are the biases used to model the measurement errors. These are the sensors calibration parameters obtained by estimation. The velocity components along the three body-fixed axes at an off-CG location are computed from u, v and w as follows:

$$\begin{aligned}
u_{offcg} &= u - (r_m - \Delta r)y_{offcg} + (q_m - \Delta q)z_{offcg} \\
v_{offcg} &= v - (p_m - \Delta p)z_{offcg} + (r_m - \Delta r)x_{offcg} \\
w_{offcg} &= w - (q_m - \Delta q)x_{offcg} + (p_m - \Delta p)y_{offcg}
\end{aligned} \quad \ldots (29)$$

where (x_{offcg}, y_{offcg}, z_{offcg},) denote the offset distances from the centre of gravity to the flow angle sensor mounted on the aircraft; (u_{vane}, v_{vane}, w_{vane}) are the velocity components along the three body-fixed axes corresponding to the flow angle sensor-vane deflection; (u_{spb}, v_{spb}, w_{spb}) and (u_{npb}, v_{npb}, w_{npb}) are the velocities components corresponding to side airdata pressure probe and nose pressure probe respectively. From the postulated system dynamic and measurement models (26-28), state, input, measurement and parameter vectors are, respectively.

$$\begin{aligned}
x &= \begin{bmatrix} u & v & w & \phi & \theta & h \end{bmatrix}^T \in \Re^6; u = \begin{bmatrix} A_x & A_y & A_z & p & q & r \end{bmatrix}^T \in \Re^6; \\
z &= \begin{bmatrix} V_m & \bar{q}_m & \phi_m & \theta_m & h_m & \alpha_{vane} & \alpha_{spb} & \beta_{spb} & \beta_{npb} \end{bmatrix}^T \in \Re^9; \\
\Theta &= \begin{bmatrix} \Delta p & \Delta q & \Delta r & \Delta A_x & \Delta A_y & \Delta A_z & \Delta\bar{q} & \ldots \\ K_{\alpha_{vane}} & \Delta\alpha_{vane} & K_{\alpha_{spb}} & \Delta\alpha_{spb} & K_{\beta_{spb}} & \Delta\beta_{spb} & K_{\beta_{npb}} & \Delta\beta_{npb} \end{bmatrix}^T \in \Re^{15};
\end{aligned} \quad \ldots (30)$$

Finally, the KF extended state vector is defined as

$$\begin{bmatrix} u & v & w & \phi & \theta & h & \Delta p & \Delta q & \Delta r & \Delta A_x & \ldots \\ \Delta A_y & \Delta A_z & \Delta\bar{q} & K_{\alpha_{vane}} & \Delta\alpha_{vane} & K_{\alpha_{spb}} & \Delta\alpha_{spb} & K_{\beta_{spb}} & \Delta\beta_{spb} & K_{\beta_{npb}} & \Delta\beta_{npb} \end{bmatrix}^T \in \Re^{21} \quad \ldots (31)$$

4.1 Turbulence model

In case of flight in turbulence, estimated flow angles using above-mentioned state and measurement equations show major variation from simulated flight values. It is mainly due to the model deficiency in the estimation framework. Dynamical representation of atmospheric turbulence is obtained by including Dryden model in the system equations used for estimation. The features that distinguish one turbulence structure from the other are the turbulence intensity α and integral scale of turbulence L. In the present investigation L = 1,750ft and σ =10ft/sec are considered to generate moderate turbulence condition. To account for turbulence in forward velocity, lateral velocity and vertical velocity, the dynamic model considered and appended to the state model in (33) has the following form[29]:

$$\begin{aligned}
\dot{y}_u &= \frac{-y_u + x_u k_u\sqrt{\frac{\pi}{\Delta t}}}{t_u} \\
\dot{y}_{v_2} &= y_{v_1} \\
\dot{y}_{v_1} &= -\frac{y_{v_2}}{t_v^2} - \frac{2y_{v_1}}{t_v} + x_v\sqrt{\frac{\pi}{\Delta t}} \\
\dot{y}_{w_2} &= y_{w_1} \\
\dot{y}_{w_1} &= -\frac{y_{w_2}}{t_w^2} - \frac{2y_{w_1}}{t_w} + x_w\sqrt{\frac{\pi}{\Delta t}}
\end{aligned} \quad \ldots (32)$$

where x_u, x_v, x_w random numbers are generated to simulate the random nature of turbulence; t_u, t_v, t_w k_u, k_v, and k_w are the time constants that are defined as follows:

https://doi.org/10.1017/S0001924000005509 Published online by Cambridge University Press

Table 1
Measurement noise levels used in simulated data

Sensor	Standard deviation, σ	unit
Accelerometers	0·01	m/s^2
Rate gyros	0·0001	rad/s
Alpha measurement-1	0·0003	rad
Alpha measurement-2	0·0002	rad
Bata measurement	0·0008	rad
Vertical position	0·012	metre
Dynamic pressure	10	Pa
Euler angles	0·0002	rad
True airspeed	0·01	m/s

$$t_u = \frac{L_u}{V_t}, t_v = \frac{L_v}{V_t}, t_w = \frac{L_w}{V} \text{ where } V_t = \sqrt{u^2 + v^2 + w^2}, \sigma_u = \sigma_v = \sigma_w = \sigma;$$

$$L_u = L_v = L_w = L; \quad k_u = \sqrt{\frac{\left(2\sigma_u{}^2 t_u\right)}{\pi}}; \quad k_v = \sqrt{\frac{\left(2\sigma_v{}^2 t_v\right)}{\pi}}; \quad k_w = \sqrt{\frac{\left(2\sigma_w{}^2 t_w\right)}{\pi}}$$

The turbulence in velocity components in flight path axes can now be obtained using the relations[29]:

$$u_{fturb} = y_u, \; v_{fturb} = \frac{k_v}{t_v}\left[\frac{y_{v_2}}{t_v} + \sqrt{3}\cdot y_{v_1}\right] \text{ and } w_{fturb} = \frac{k_w}{t_w}\left[\frac{y_{w_2}}{t_w} + \sqrt{3}\cdot y_{w_1}\right]$$

Turbulence generated in flight path axes transformed to body axes are given by

$$\begin{bmatrix} u_{bturb} \\ v_{bturb} \\ w_{bturb} \end{bmatrix} = \begin{bmatrix} \text{Cos}(\alpha)\text{Cos}(\beta) & -\text{Cos}(\alpha)\text{Sin}(\beta) & -\text{Sin}(\alpha) \\ \text{Sin}(\beta) & \text{Cos}(\beta) & 0 \\ \text{Sin}(\alpha)\text{Cos}(\beta) & -\text{Sin}(\alpha)\text{Sin}(\beta) & \text{Cos}(\alpha) \end{bmatrix} \begin{bmatrix} u_{fturb} \\ v_{fturb} \\ w_{fturb} \end{bmatrix} \quad \ldots (36)$$

$$\text{where} \beta = \text{Sin}^{-1}\left(\frac{v}{V_t}\right) \text{ and } \alpha = \text{Tan}^{-1}\left(\frac{w}{u}\right)$$

In the influence of turbulence, the equations relating the states in x to the measurement z in Equation (26) are modified through replacing u, v and w by $u - u_{bturb}$, $v - v_{bturb}$ and $w - w_{bturb}$ in Equation (28) respectively.

5.0 EXPERIMENTAL RESULTS

In this section the proposed multi sensor data fusion method is validated via a FPR application using both simulated data with wind/turbulence effects, generated through nonlinear simulation software and flight test data obtained from a high performance fighter aircraft prototype flight test. The measurement and process noise covariance matrices are design parameters for the Kalman filter, which were calculated from existing time histories through data filtering.

5.1 Simulated data results

The simulated data for pitch stick and rudder doublet inputs were generated at flight condition of Mach 0·3, altitude 1,800 metres, with 15m/sec steady winds at various heading angles (0°, 90°, 180°, 270°) and also for moderate turbulence. Simulated data were corrupted by a time varying input and measurement noise with typical signal to noise levels found in real applications (see Table 1). The simulated data were generated at a sampling rate of 0·025sec.

For the sake of defining measurements in simulation AOA and AOSS are computed using the following equations. These measurements are influenced by wind/ turbulence also.

$$\alpha_{m1} = \text{Sin}^{-1}\left(\frac{\text{Sin}\theta_m}{\sqrt{\text{Sin}^2\theta_m + \text{Cos}^2\theta_m\text{Cos}^2\phi_m}}\right)$$

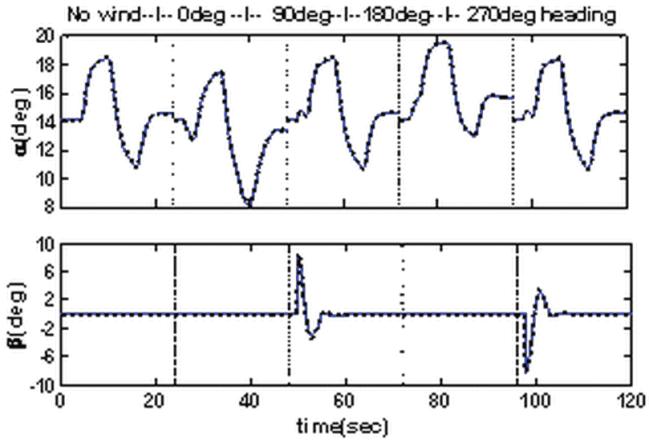

Figure 4. Comparison of estimated and flight simulated Responses: ——— Flight simulated and - - - - -, estimated. [Pitch stick doublet with 15m/s wind at various heading angles]

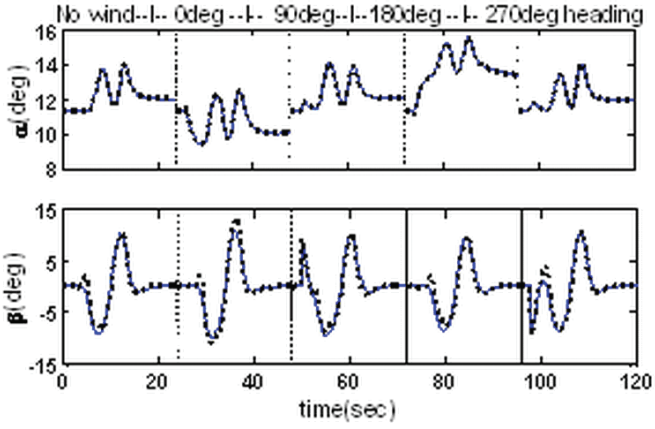

Figure 5. Comparison of estimated and flight simulated Responses: ———— Flight simulated and - - - - -, estimated. [Rudder doublet with 15m/s wind at various heading angles]

$$-\text{Sin}^{-1}\left(\frac{\frac{\dot{h}_m}{V_m} + \text{Sin}\beta_m\text{Sin}\phi_m\text{Cos}\theta_m}{\left(\sqrt{\text{Sin}^2\theta_m + \text{Cos}^2\theta_m\text{Cos}^2\phi_m}\right)\text{Cos}\beta_m}\right)$$

where $\dot{h}_m = (u-u_g)\,\text{Sin}\theta_m - (v-v_g)\,\text{Sin}\phi_m\,\text{Cos}\theta_m - (w-w_g)\,\text{Cos}\phi_m\,\text{Cos}\theta_m$

$$V_m = \sqrt{(u-u_g)^2 + (v-v_g)^2 + (w-w_g)^2}$$

$$\alpha_{m2} = \frac{\frac{m\cdot A_z}{\bar{q}\cdot S} - C_{z_0}}{C_{z_\alpha}} \quad \ldots (37)$$

$\beta_m = -A_{y\beta gain})A_y$, where $A_{y\beta gain}$ is A_y to β gain and is taken from the look up table given as a function of dynamic pressure ($\bar{q}$).

The reconstructed AOA and AOSS from estimated states are obtained by applying KF Technique to each of the data sets with $15ms^{-1}$ wind at various heading angles. Here, we have introduced initial state $\mathbf{x_0}$ = (99·67587, –0·0196, 25·009, 0·0001, 0·24585, 1,800) and state propagation error covariance matrix $\mathbf{P_0}$= diag (100·429, 15, 120·58, 20, 2·0028, 2,500). These estimated responses of α and β compare well with the simulated flight data A typical estimation result for the case of EKF based measurement fusion method (MF-I) is shown in Figs 4 and 5. The Calibration parameters of AoA are noted in average as K_α = 0·9611,

https://doi.org/10.1017/S0001924000005509 Published online by Cambridge University Press

Table 2
Performance comparison study based on simulated data with wind effects

Mean parameter	EKF			UKF		
	MF-1	MF-1I	SVF	MF-1	MF-1I	SVF
Time-taken	0·2626	0·05	0·1725	0·2626	0·05	6·5853
% fit error α	0·131	0·172	0·1551	0·131	0·172	0·08629

Table 3
Performance comparison study based on simulated data with turbulence effects

Mean parameter	EKF			UKF		
	MF-1	MF-1I	SVF	MF-1	MF-1I	SVF
Time-taken	2·5008	1·0628	2·1443	14·5958	8·2121	12·9959
% fit error α	0·10415	2·34125	1·70286	0·0939	1·7936	1·14428

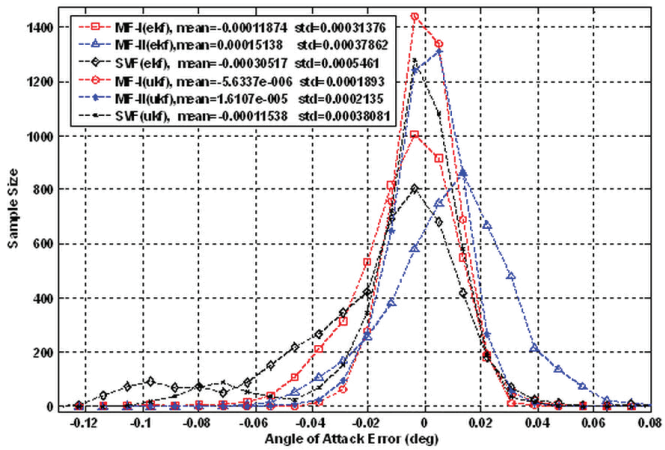

Figure 6. Error analysis of AOA based on multi sensor data fusion.

$\Delta\alpha = 0{\cdot}197$ deg for pitch stick doublet and $K_\alpha = 1{\cdot}1896$, $\Delta\alpha = -2{\cdot}223$deg for rudder doublet.

In the case of turbulence, the nominal set of kinematic state equations used in the KF is not sufficient to extract the entire information from the data. Therefore, investigations are made with turbulence model included in the estimation framework. The estimated responses of the flow angles obtained by applying KF to the data sets having wind or turbulence effects compare well with the simulated flight data.

The performance comparison of multi sensor data fusion approaches, which are discussed in Section 3, applied to simulated data with wind and turbulence are given by Table 2 and 3 respectively.

It is noted that MF-I performs better in terms of accuracy in estimation but computational time is more, whereas MFII is computationally effective for the cost of performance compared to other sensor fusion methods. The mean AOA error value of MFII is away from zero value indicates its performance reduction as shown in Fig 6. It is observed that sample size for AOA error in UKF is high and its

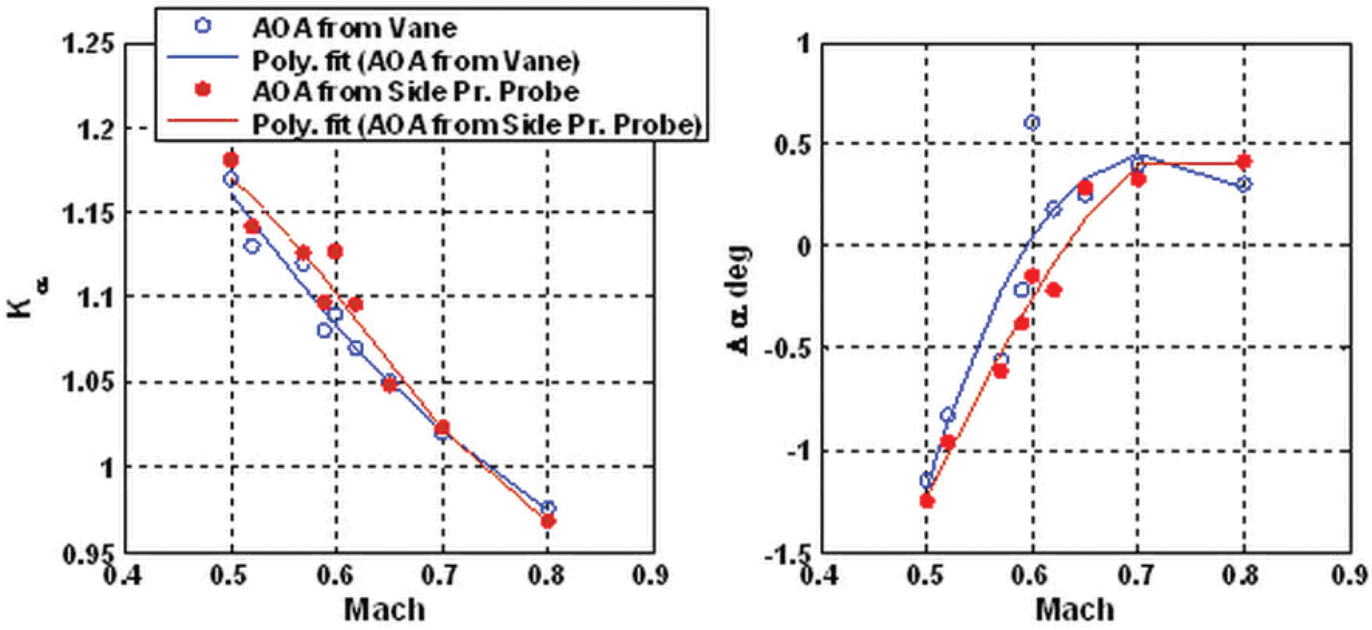

Figure 7. Filter estimated AOA calibration parameters.

https://doi.org/10.1017/S0001924000005509 Published online by Cambridge University Press

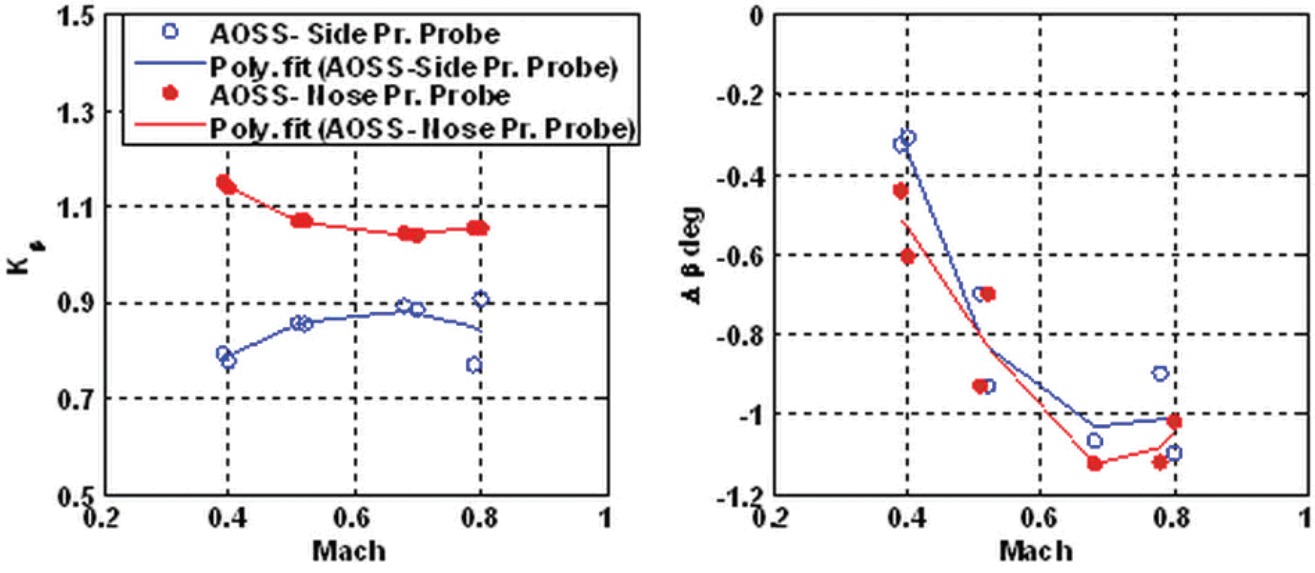

Figure 8. Filter estimated AOSS calibration parameters.

error standard deviation always less than EKF. Therefore, UKF always has better performance over EKF, but computational time is more due to the state augmentation through process and measurement noise. SVF shows good performance with normal computational complexity. As it is fault tolerant and computationally effective, SVF has great value in online practice.

5.2. Flight test data results

To evaluate the proposed data fusion method in a real condition, high performance fighter aircraft prototype was used to generate the data necessary for the analysis. Dynamic manoeuvres (doublets, 3211, pull up and AOA sweep) for the variation of mach from 0·39 to 0·95 and altitude from 2,000 to 14,000 metres, AOA excursions up to 21° and AOSS excursions up to ±5° were selected. The sampling period adopted was 0·025 second. It is required to validate the sensor data fusion approach by comparing with standard technique OEM for FPR using ESTIMA software package[21]. The OEM is successively applied to estimate the sensitivity factor and bias of calibration parameters for the multi sensors and use to correct the measurements AOA and AOSS. The corrected AOA and AOSS values are to be used as references; the filter results are compared against calibrated data based on reference method OEM[7]. The application of OEM for FPR using ESTIMA is omitted here for brevity. It is worth noting that proposed flow angle sensors are dissimilar since AOA senses by different sensors vane and pressure probe, while AOSS senses by nose pressure probe and side airdata pressure probe. In such case, MF-II is not applicable to use. Therefore, MF-I and SVF are applied to estimate flow angles from the flight test data. The analysis of flight manoeuvres for various Mach numbers were carried out separately mainly because, from *a priori* knowledge, the sensitivity factor is expected to vary with speed. Figures 7 and 8 show variation of sensitivity factors and offset errors estimated for flow angles separately from manoeuvres at different Mach numbers. It is observed that correction factors for AOA show a clean reduction for higher values of Mach numbers. The difference between AOA, AOSS estimated using sensor fusion based approaches and those obtained using ESTIMA is shown in Fig. 9.

The variation of estimation errors of alpha and beta are respectively, almost around aerospace industry requirement values deg and deg for the MF-I except at some certain points. The larger error in AOA and AOSS at these points is due to mismatch in the initial values of the manoeuvres. Of course this initial value problem does not arise for the online application of KF based sensor fusion algorithm. Even though the performance of SVF is not as good as measurement fusion, it can improve by introducing more number of accurate sensors for fusion and it is greater value in online practice as having the property of fault tolerant and less computational complexity.

6.0 CONCLUSION

EKF and UKF based various multi sensor data fusion methods were applied to dynamic manoeuvres to calibrate the AOA and AOSS in real time from both simulated and real flight data of a high performance aircraft. Simulations in software were carried out with 15m/sec wind effects at 1,800 metres altitude and 0·3 Mach to obtain sufficient variations in α,β of the aircraft. The investigations were initially made using simulated data with wind and turbulence effects and it was shown both AOA and AOSS estimates were accurate. The same procedure was extended to real time flight test data of a high performance aircraft. It is observed that UKF is superior to EKF in terms of accuracy of estimation as it equivalently captures the effects of nonlinearities up to second order without the need for explicit calculations of the Jacobians. Among all the sensor fusion techniques, MF-I performs better estimation accuracy of about ±0·5° and ±0·25°, respectively for AOA and AOS. SVF is of a greater value for online implementation because it is more fault-tolerant and less computationally complex. In addition, OEM for FPR using ESTIMA was applied to the same dynamic manoeuvres to calibrate the airdata sensors. The consistently good results obtained using sensor data fusion techniques proposed in this paper establish that these techniques are of great value for online implementation.

ACKNOWLEDGMENTS

The authors are grateful to Amitabh Saraf, Scientist-F, ADA, Bangalore and Jatinder Singh, Scientist-F, NAL, Bangalore for their encouragement and technical discussion during the course of work. The authors also gratefully acknowledge Shyam Chetty, Head, Flight Mechanics and Control Division of National Aerospace Laboratories, Bangalore for his moral support.

https://doi.org/10.1017/S0001924000005509 Published online by Cambridge University Press

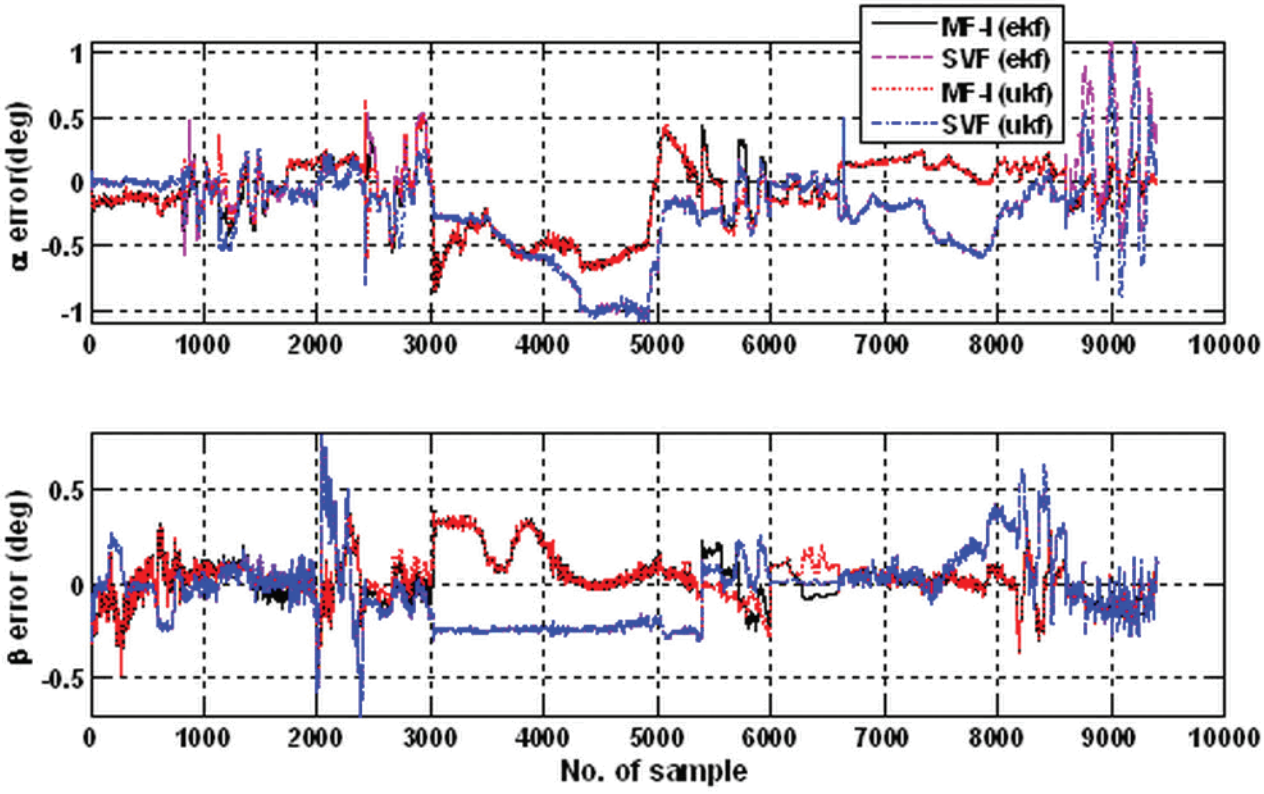

Figure 9. Filter estimated errors of AOA and AOSS.

REFERENCES

1. MENZIES, M.A. Integrated air data sensors, *Aeronaut J*, **105**, (1046), April 2001, pp 223-229.
2. PARAMESWARAN V, JATEGAONKAR R.V. and PRESS, M. Five-hole flow angle probe calibration from dynamic and tower flyby maneuvers, *J Aircr*, **42**, (1), January–February 2005.
3. EDWARD, A and HAERING. Air data measurement and calibration, December 1995, NASA-TM 104316.
4. GONSALEZ J.C. and ARRINGTON, E.A. Five-hole flow angle calibration for the NASA Glenn icing research tunnel, NASA/CR-1999-202330, AIAA–96–2201.
5. STEPHEN. A. and TERRY. J. High angle-of-attack flush airdata sensing system, *J Aircr*, 1992, **29**, (5), pp 915–921.
6. LANDO, M., MANUELA and PIERO, Neuro-fuzzy techniques for the air-data sensor calibration, *J Aircr*, **44**, (3), May-June 2007.
7. CHU Q.P., MULDER. JA. and VAN WOERKOM, P.T.L.M. Modified recursive maximum likelihood adaptive filter for nonlinear aircraft flight-path reconstruction, *AIAA J*, Guidance Control Dyn, 1996; **19**, (6), pp 1285-95.
8. KLEIN, V. and SCHIESS, J.R. Compatibility check of measured aircraft responses using kinematic equations and extended Kalman filter, August 1977, NASA TN D-8514.
9. JATEGAONKAR, R.V. Identification of the aerodynamic models of the DLR research aircraft ATTAS from flight test data, July 1990, DLR, German Aerospace Center, Rept DLR-FB 90-40, Brunswick, Germany.
10. KESKAR, D.A. and KLEIN, V. Determination of instrumentation errors from measured data using maximum likelihood method, 1980, AIAA 80-1602.
11. MAINE, R.E., and ILIFF, K.W. Identification of dynamic systems applications to aircraft Part 1: The output error approach, December 1986, AG-300, AGARD, **3**, (1).
12. LABAN, M.,On-line Aircraft Aerodynamic Model Identification, 1994, PhD Dissertation, Delft University of Technology, Delft, Netherlands.
13. DE BRAGA, C.M., MOREINA, E.H. and CARLOS L.S.G. Adaptive stochastic filtering for online aircraft flight path reconstruction, *J Aircr*, September-October 2007, **44**, (5).
14. FITZGERALD, R.J. Divergence of the Kalman fFilter, *IEEE Transactions on Automatic Contro*l, 1971, **AC-16**, (6), pp 736–747.
15. JULIER, S. and UHLMANN, J.K. Unscented filtering and nonlinear estimation, *Proceedings of the IEEE*, March 2004, **92**, pp 401-422.
16. WISE, K.A. Flight testing of the X-45 A J-UCAS computational Alpha-Beta system, 2006, AIAA 2006-6215.
17. HALL, D.L. *Mathematical Techniques in Multi Sensor Data Fusion*, 1992, 1st edition, Artech House, Norwood.
18. BAR-SHALOM,Y. and FORTMANN, T.E. *Tracking and Data Association*, 1998, Academic Press, New York.
19. SAHA, R.K. Track-to-track fusion with dissimilar sensors, *IEEE Transactions on Aerospace and Electronic Systems*, 1996, **34**, (3), pp 1021-1029.
20. HUI, K., SRINIVASAN, R. and BAILLIE, S. Simultaneous calibration of aircraft position error and airflow angles using differential GPS, *Canadian Aeronautics and Space J*, December 1996, **42**, (4), pp 185-193.
21. JATEGAONKAR, R.V. ESTIMA — a modular and integrated software tool for parameter estimation and simulation, July 2001, DLR, German Aerospace Center, IB 111-2001/29, Brunswick, Germany.
22. HAMEL, P.G. and JATEGAONKAR, R.V. Evolution of flight vehicle system identification, *J Aircr*, 1996, **33**, (1), pp 9–28.
23. MAYBECK, P.S. *Stochastic Models, Estimation, and Control*, Vol 1, 1979, Academic Press, New York.
24. JATEGAONKAR, R.V. Flight vehicle system identification: A time domain methodology, August 2006, **216**, AIAA Progress in Astronautics and Aeronautics Series, AIAA, Reston, VA.
25. GAN, Q. and HARRIS, C.J. Comparison of two measurement fusion methods for Kalman-filter-based multi sensor data fusion, *IEEE Transactions on Aerospace and Electronic Systems*, January 2001, **37**, (1).
26. ROECKER, J.A. and MCGILLEM, C.D. Comparison of two sensor tracking methods based on state-vector fusion and measurement fusion, *IEEE Transactions on Aerospace and Electronic Systems*, **24**, (4), 1988, pp 447-449.
27. CHANG, K.C., SAHA, R.K. and BAR-SHALOM, Y. On optimal track-to-track fusion, *IEEE Transactions on Aerospace and Electronic Systems*, 1997, **33**, (4), pp 1271-1276.
28. SAHA R.K. Effect of common process noise on two-track fusion, *J Guidance, Control Dynamics*, 1996, **19**, pp 825-835.
29. MARVIN, J.G. A perspective on CFD validation, 1993, Dryden Lectureship in Research, AIAA-1993-2, 31st Aerospace Sciences Meeting, 11-14 January 1993, Reno, NV.

https://doi.org/10.1017/S0001924000005509 Published online by Cambridge University Press